

Quarterly Report

Date of report: January 22, 2008

For quarter ending: December 31, 2007

Agreement number: DTPH56-06-X-000029

Agreement Time period: June 30, 2006 to June 29, 2008

Project: Mechanical Properties and Crack Behavior in Line Pipe Steels

Prepared by: NIST, Materials Reliability Division, Boulder, CO

Project Tasks:

Task 1: Fatigue crack growth

Task 2: Hydrogen charged fatigue crack growth

Task 3: CTOA testing and modeling

Task 4: Fracture surface examination

Task 5: Method for determination of yield strength in high strength pipeline steels and welds

Task 6: Other tasks as assigned

Task 7: Reporting

NIST-Boulder received the contract for this program in early June 2006. Our efforts are focused on CTOA testing of pipeline steels, weldments and heat affected zones (girth and seam), and the development of a model for our dynamic ductile fracture experiments. Most of our efforts this past quarter were concentrated on reducing data generated during the quasi-static and dynamic rate CTOA tests. In addition, full-thickness transverse and axial orientation fatigue experiments are under way and the hydrogen charged tests have been completed.

The following task updates should be appended to previously submitted quarterly reports.

Technical status of tasks:

Task 1: Fatigue crack growth

The axial fatigue tests continue at $r=0.1$ and 0.4 . The axial specimen (M(T) geometry) testing is almost complete and we plan to finish this portion of the effort early this quarter. The uneven fatigue crack propagation through the pipe wall thickness in a couple of the specimens has prompted us to investigate this phenomenon further. We ordered software that will allow us to monitor and record the fatigue crack growth on both the ID and the OD of the pipe wall, enabling us to better understand this uneven crack growth.

The software arrived at the end of the last quarter and we found that further modifications to the controller were needed to conduct these tests as planned. The parts for the modification have been ordered and should arrive in the next week. These tests (axial) were machined such that fatigue data was generated in only the transverse (circumferential) direction. We machined pipeline specimens in the compact tension (C(T)) geometry for longitudinal crack fatigue testing and have started those tests. They should be complete early this quarter. Initial C(T) specimen were machined and tested in the transverse direction in order to verify data in the different geometry with the axial M(T) fatigue specimens.

In addition to the experimental work described above, a model is being developed that can help describe the influence of the pipe curvature on fatigue properties. This work, described below, will continue into the next quarter and will be reported on as progress warrants.

Fatigue Modeling

M(T) Specimen Models

To supplement the fatigue modeling work discussed in the last quarterly report, an expression to relate the CMOD results for a curved Middle Tension, M(T), specimen to the results to a flat M(T) expression was developed. As discussed before, the American Society of Testing Materials (ASTM) expression for crack length as a function of the compliance (CMOD/Load) inaccurately predicted the crack length for both the curved and flat specimen finite element models as shown in figure 1 for X65 steel.

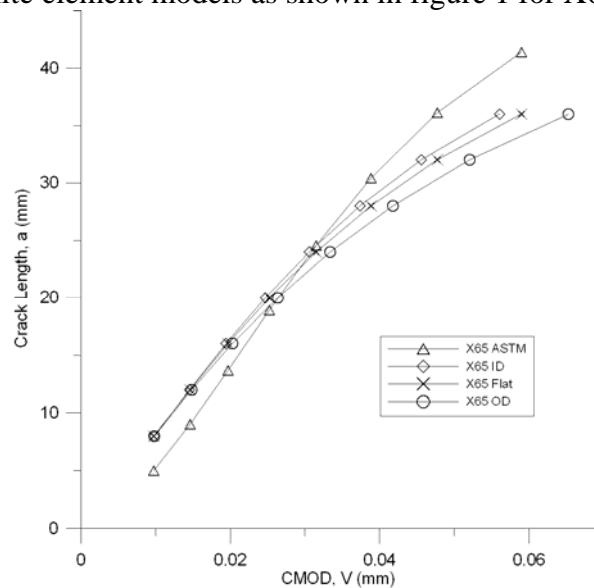


Figure 1. Comparison of FE results to ASTM prediction, X65

However, the Eftis and Liebowitz expression much more accurately predicted the crack length for the flat specimen as shown in figure 2 for the X100, X65 and Grade B geometries.

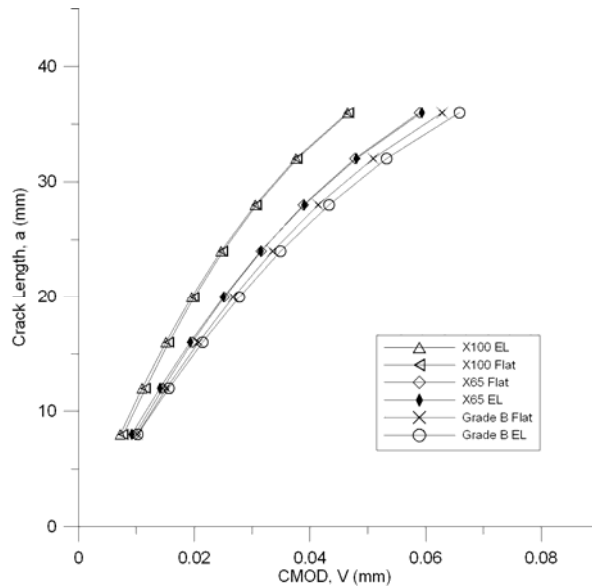


Figure 2. Weight Function results compared to flat

By developing a relationship between the curved and flat CMOD results from the models, it would then be possible to use the Eftis and Liebowitz expression to predict the crack length for curved specimens without having to modify the expression itself.

To develop the relation between the curved and flat CMOD values, four different actual curved M(T) test specimen geometries were constructed. Additional models with varying thickness, curvature, and load were also constructed to verify that the relation was valid over a wide variety of specimen configurations—nineteen different models in total.

It was found that the very simple relationship to relate the curved results to the flat results was valid for all of the different scenarios:

$$CMOD' = W_{OD} \cdot CMOD_{OD} + W_{ID} \cdot CMOD_{ID} \quad (1)$$

where $CMOD'$ is the corrected CMOD results and $W_{OD} = 0.2$ and $W_{ID} = 0.8$ are weighting factors. This relationship is very easy to use and shows a good crack length prediction. Further investigations are in progress in order to evaluate directly the crack length from the ID or OD CMOD measurement. These results will be shared with the ASTM Committee E08 so that they might consider it for future revisions to the standard.

C(T) specimen models

Because of the large discrepancy between the ASTM expression for crack length as a function of compliance for the flat M(T) specimens, a finite element model of the compact tension C(T) specimen was also constructed so that the ASTM C(T) expression could be validated. Figure 3 shows the finite element model of the C(T) specimen, and

figure 4 shows the comparison of the ASTM crack length-compliance expression and the finite element results.

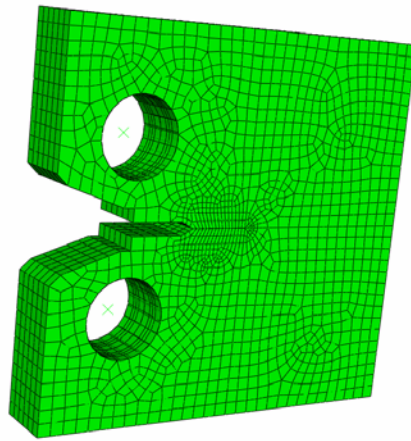


Figure 3. Finite element model of C(T) specimen.

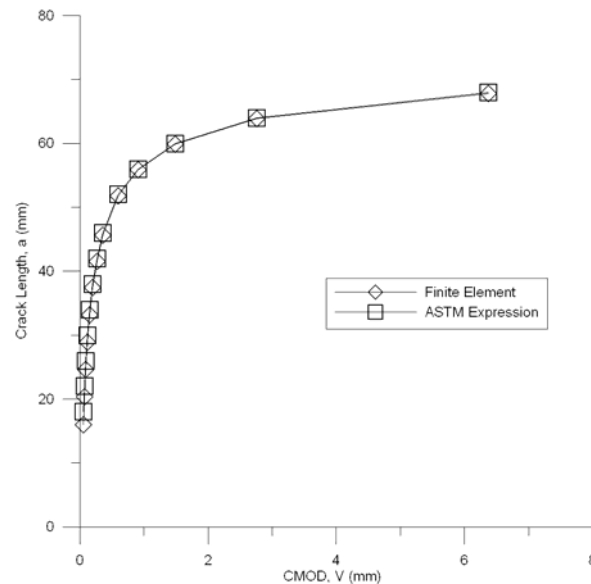


Figure 4. Comparison of the crack vs. compliance for the ASTM expression and finite element results.

From the figure, it is clear that the ASTM expression for the C(T) specimen is considerably more accurate than the expression for the M(T) geometry. While at the smallest crack length examined (18mm for this particular geometry) an under prediction of 11% exists, as the crack length increases the difference between the model and the ASTM prediction decreases to nearly zero. Because of this small error, the ASTM C(T) expression was taken to be valid. Additionally, since the C(T) specimen is small, it can be machined flat from within the pipe thickness and unlike the M(T) specimen, no corrections for the pipe curvature need to be considered.

Comparison of M(T) and C(T) test results

However, the M(T) specimen is more commonly used to examine the fatigue crack growth rate and the C(T) specimen is traditionally used for fatigue crack threshold studies and fracture toughness determinations. To explore whether there is any difference in the fatigue crack growth rates by using the different specimens, C(T) tests were run in conjunction with the M(T) tests. Figure 5 shows a comparison of the results for the C(T) and M(T) specimens for X100 steel. The figure shows that the results are very similar for both types of specimens.

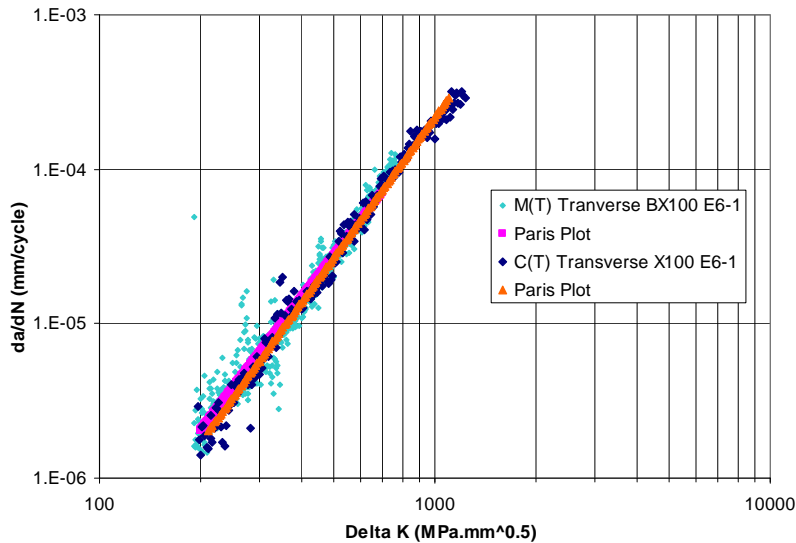


Figure 5. Comparison of M(T) and C(T) specimen FCGR results with crack growth in the transverse direction for X100.

In addition to the C(T) specimens oriented with the crack growth in the transverse direction, tests were also run with the C(T) specimen oriented so that the crack growth was in the longitudinal direction. The results of this test compared to the M(T) results in the transverse direction are shown in figure 6.

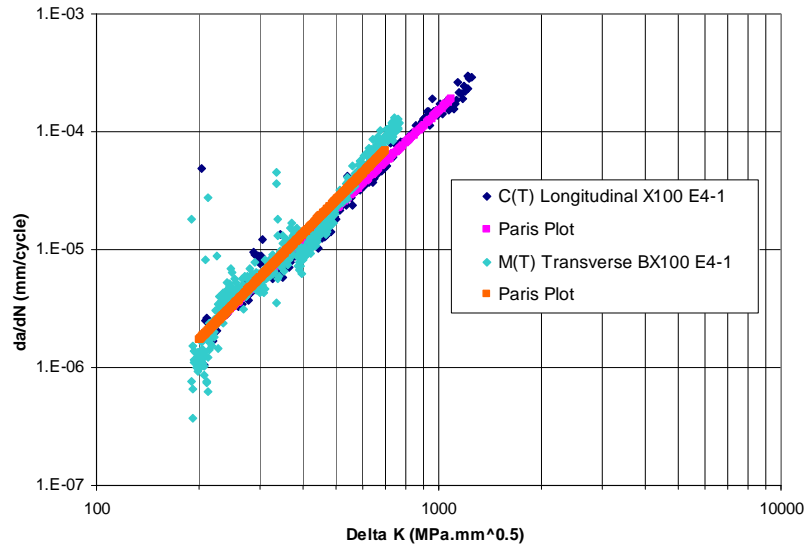


Figure 6. Comparison of FCGR results of C(T) specimen in longitudinal direction and M(T) specimen in transverse direction for X100.

From the figure, a slight difference in the results between the longitudinal and transverse direction is seen. This is most likely due to the anisotropic behavior of X100 due to the UOE forming process it undergoes; however, further analysis of the results is in progress. The apparent anomalous data points in the M(T) specimen data were generated during a few stop/restart cycles due to power outages.

While the two figures above suggest that the C(T) and M(T) specimens produce similar FCGR results for X100, Figures 7 and 8 showing the test results of X65 grade steel suggest otherwise. Comparing the results with the crack growth in the transverse direction for both in figure 7, considerable differences between the two specimen results can be seen.

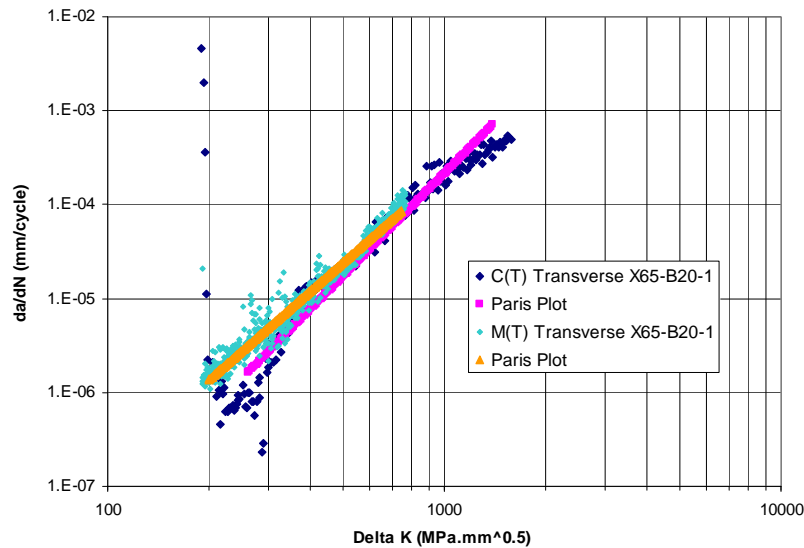


Figure 7. Comparison of M(T) and C(T) specimen FCGR results with crack growth in the transverse direction for X65.

However, a plot of the results for the C(T) specimen orientated so that the crack growth is in the longitudinal direction with the M(T) in the transverse direction is shown in figure 8. From the figure, little difference between the longitudinal and transverse FCGR data is seen.

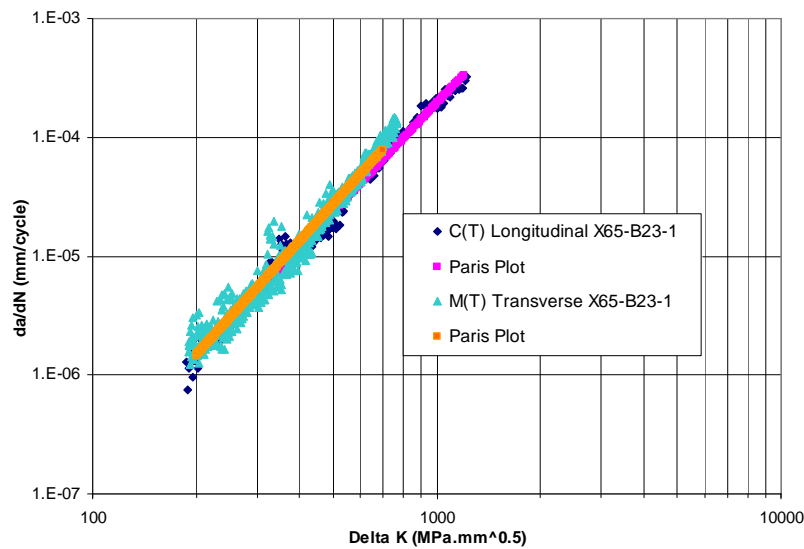


Figure 8. Comparison of FCGR results of C(T) specimen in longitudinal direction and M(T) specimen in transverse direction for X65.

The two figures above suggest that the differences between the C(T) and M(T) results may be more a result of the variability of the material properties than the specimen geometries or crack orientations. Further analysis is being performed to better understand the differences.

X100 GIRTH WELD MATERIAL PROPERTIES:

To better understand the fracture properties (dynamic and quasi-static) of the high strength pipeline steels, we needed reference data on the base metal, heat-affected zone and weld metal interactions. The previous two quarterly reports summarized these findings and some of that information is repeated here for comparison purposes with the latest generated data. This quarter, we ran tensile tests on all-weld-metal removed from the girth weld of the X100 pipeline material.

API X100 high strength grade pipeline steel (outside diameter 52 inch (1.32 m) and wall thickness 20.6 mm) was investigated. Table A contains the nominal chemical composition of this steel (weight %).

Table A. Chemical composition of the X100 tested steel (weight %)

C	Mn	P	S	Si	Ni	Cu	Mo
0.07	1.90	0.008	0.0005	0.10	0.50	0.30	0.15

To measure the tensile properties of the pipeline base metal, weld and HAZ, round tensile specimens were machined in both axial (longitudinal) and transverse orientations.

The girth weld was made by use of the shielded metal arc (manual) process for the fill and cap. The root welding electrodes are not specified here.

To characterize the weld section, micro hardness measurements and tensile tests were performed throughout the weld section. Round tensile specimens were machined in the axial (longitudinal) direction, across the weld, with the girth weld and HAZ included in the gauge length (see Figure 9), creating a “composite” tensile test. An extensometer was used to measure the global elongation of the weld and the two HAZ, and a strain gauge was used to measure the local deformation of the weld.

All experiments were performed in either a screw-driven tensile testing machine of 100 kN capacity, or a closed-loop servo-hydraulic machine of 100 kN capacity. Tests were conducted in displacement control at a rate of 0.1 mm/min.

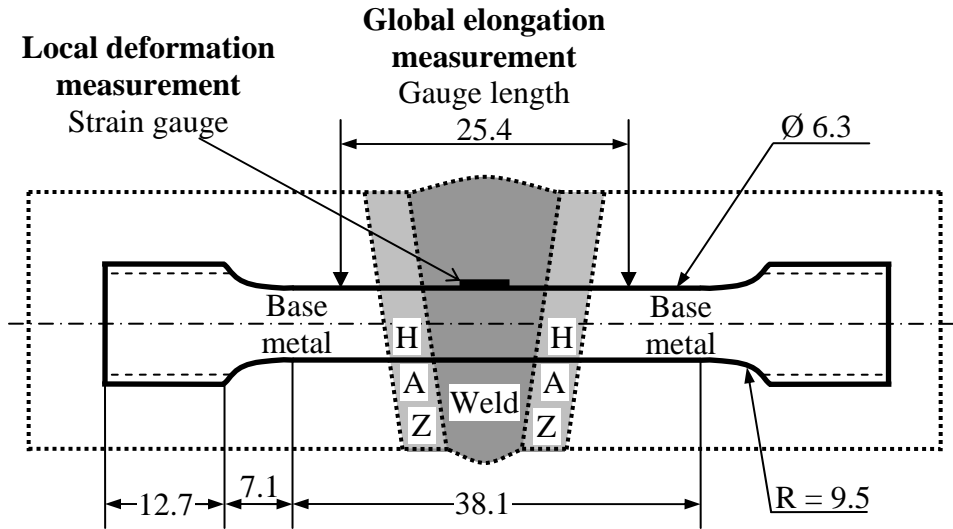


Figure 9. Round tensile specimen across the girth weld section (dimensions in mm).

A summary of the tensile properties of the base metal and the weld is shown in Table B, where $\sigma_{0.2}$ is the yield stress, σ_{UTS} is the ultimate strength, e_u is the uniform elongation, and e_f is the failure elongation.

Table B. Tensile mechanical properties of the base metal and the girth weld

Orientation	$\sigma_{0.2}$ (MPa)	σ_{UTS} (MPa)	$\sigma_{0.2}/\sigma_{UTS}$	e_u (%)	e_f (%)	e_u/e_f
Base Metal Transverse	798	827	0.97	4.1	19.3	0.21
Base Metal Longitudinal	732	806	0.91	4.6	20.3	0.23
Global Girth Weld	602	717	0.84	3.9	11.4	0.35

Figure 10 presents the tensile test results for the base metal, longitudinal and transverse directions, and for the girth weld (global (weld plus HAZ) and local (weld only)).

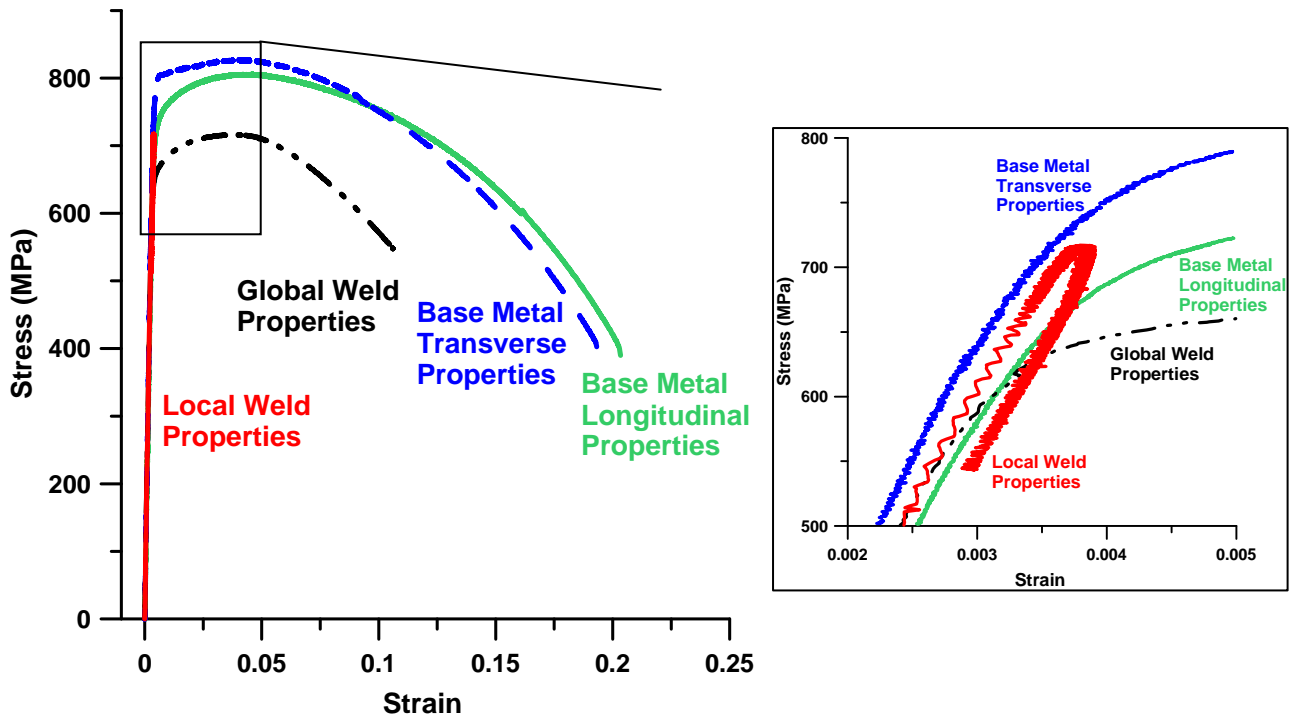


Figure 10. Base metal and girth weld tensile properties, with details for initial yielding (0.002 to 0.005 strain) shown in the expanded section.

From the “composite” tensile tests, several remarks can be made:

- The transverse orientation base metal specimens have a higher yield stress and lower uniform and failure elongation than those for the longitudinal orientation. This result is typical of the pipeline UOE (U-shape, O-shape and Expansion) forming process.
- The global girth weld data undermatches the base metal UTS, uniform elongation, and elongation to failure by 11.0 %, 15.2 % and 43.8 %, respectively. These results indicate that this manual weld is not slightly stronger (overmatched) than the base metal, as desired for pipeline service, when a large global deformation is anticipated.
- The weld (local strain measurement) is overmatched in comparison to both the global weld properties (combination of the weld and HAZ sections) and the base metal in the longitudinal direction. Unfortunately, the overmatching can not be quantified by the present tensile test technique because the strain is reduced in the weld section after reaching the UTS because of the necking (localized strain) that occurs in the HAZ near the interface of the HAZ and the base metal.

The mismatch between the weld and HAZ can be quantified by micro hardness measurements. Vickers micro hardness measurements, using a 500 g weight and a diamond point, are presented in Table C and Figure 11. The hardness measurement indicated a weld overmatch of 4 % and a 10 % under match in the HAZ.

Table C. Vickers micro hardness measurements of the girth weld section

Orientation	Vickers micro hardness measurements, using a 500 g weight and a diamond point
Base Metal Mean	272
Base Metal Standard Deviation	22
HAZ Mean	244
HAZ Standard Deviation	28
Girth Weld Mean	282
Girth Weld Standard Deviation	24

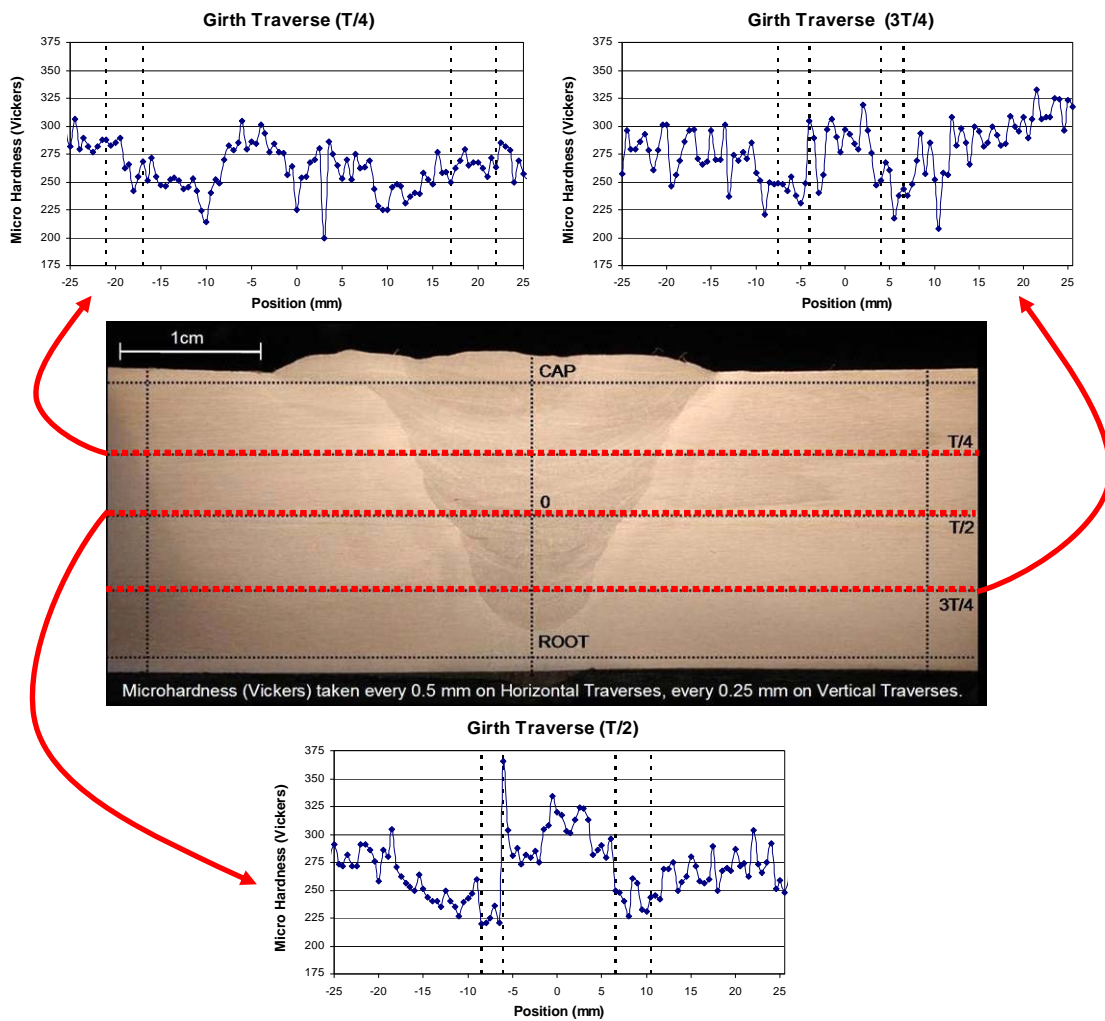


Figure 11. Girth weld section Vickers micro hardness measurements.

During this quarter, we conducted tensile tests on 3 all-weld-metal girth weld test specimens removed from the X100 pipeline. The average yield strength was 730 MPa and the average UTS was 835 MPa on the three specimens. This data confirms the earlier findings that the girth weld under-matched the base metal UTS (as well as the YS), based on these average measurements. However, weld metal testing inherently has some degree of scatter associated with the measurements and this data was no exception. The highest UTS measured on these 3 specimens was 850 MPa, making it slightly overmatching with respect to the base metal UTS. However, the other two specimens had a UTS of 717 and 714 MPa, making them undermatching. This weld was a manual weld and an automatic weld should provide more consistent results.

Task 2: Hydrogen charged fatigue crack growth

Influence of Hydrogen on Fatigue Crack Growth: Fatigue tests were performed on compact tension (C(T)) specimens in order to evaluate the influence of hydrogen (H_2) during fatigue crack propagation. The tests are complete and the data is being analyzed and will be reported on in the next quarterly report.

Task 3: CTOA testing and modeling

CTOA Testing: Quasi-static CTOA testing is complete on the girth and seam weld direction fracture specimens. Previous efforts were focused on base metals with cracks oriented in the axial direction. The current effort examines fracture resistance along the girth weld and girth heat affected zone (HAZ) as well as base metal in the girth direction. In addition, seam weld CTOA specimens have been machined to study ductile fracture resistance in the HAZ of the seam weld and weld metal, and specimens have been machined and tested with the crack propagating across the girth weld. We observed the growing crack within the seam weld material and in the direction of the weld rapidly diverted either up or down into the HAZ, not unexpectedly, as the weakest area is understood to be the adjacent HAZ. There is more scatter within and amongst tests for the CTOA associated with welds than was observed in the base metal. The 8-mm thick specimens consistently produced larger CTOA values than their 3-mm counterparts. In tests perpendicular to the girth weld, we observed occasions when the CTOA increased as an interface was approached, then drop once the interface was crossed. In relative terms, the weld had a smaller CTOA than the base metal.

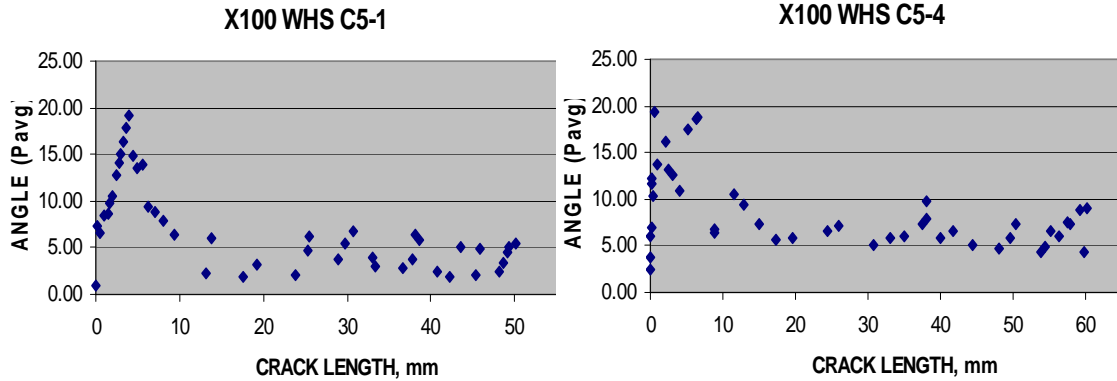


Figure 12. Data showing comparison of CTOA tests conducted in the HAZ of two specimens from the same plate of material, one 3 mm thick (left) with a mean CTOA = 4.2°, and the other 8 mm thick (right) with a mean CTOA = 6.5°.

Precracking of additional base-metal specimens is underway for the quasi-static contribution to the rate study. The dynamic testing is completed, as shown in the Table below. Both X100 and X65 MCDB CTOA specimens were tested to produce cracking rate of near 0.003, 0.03, 0.3, and 3 meters per second. Initial analysis indicates that we likely reached cracking rates of near 10 meters per second for the X100 steel.

Results for CTOA given in Table D below show the angles calculated using 3 different algorithms, which are expected to yield different, but consistent results. Differences between the X100 and X65 steels appear to be significant, when the result of a particular algorithm is compared.

Table D. Calculated CTOA angles using different algorithms.

Test Rate	X 65			X 100		
	Ct4*	P**	G***	Ct4	P	G
3 mm/sec	13.8 °	12.1 °	NA	9.7 °	8.8 °	9.5 °
30 mm/sec	12.4 °	11.0 °	16.1 °	9.2 °	8.5 °	8.6 °
300 mm/sec	12.5 °	11.3 °	11.4 °	9.2 °	7.7 °	9.7 °
Springs (3 to 10 m/s)	12.9 °	10.5 °	9.6 °	9.3 °	9.0 °	7.7 °

* Ct4 is an angle described by the crack tip and two points at the 4th position (see figure below)
 ** P is an angle calculated using several hundred points on the crack edges
 *** G is the angle calculated using points on the grid (red lines in Figure below).

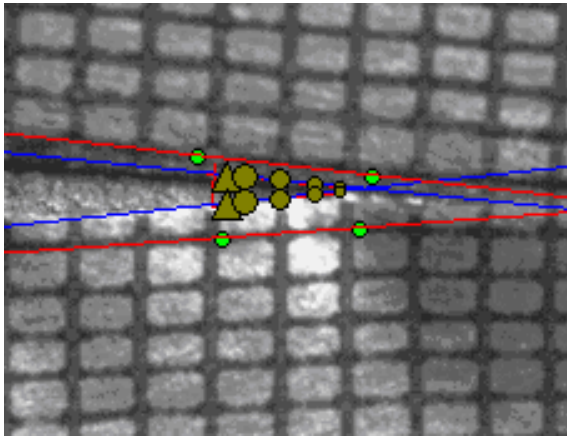


Figure 13. CTOA test evaluation for an X100 steel. The photograph was captured using a high speed camera, at a crack rate near 3 to 10 meters per second. The CTOA test was run using Belleville washers on a uniaxial test machine.

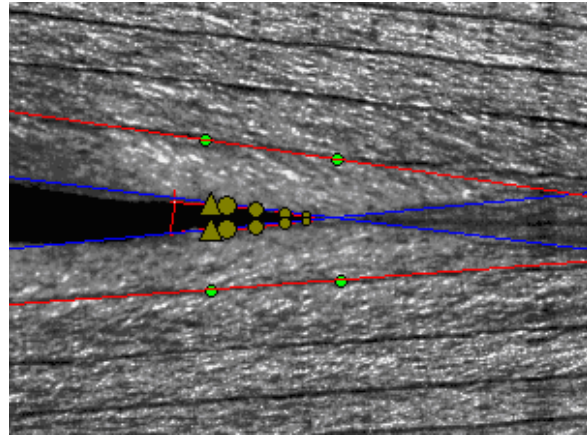


Figure 14. CTOA test evaluation for an X65 steel. The photograph was captured using a high speed camera, at a crack rate near 0.03 meters per second. The CTOA test was run on a uniaxial test machine (hydraulic).

Several examples of the dynamic testing are shown in Figures 13 and 14, above. The red line indicates the CTOA angle calculated using grid points. The blue line indicates the CTOA angle calculated using lines fitted to the profile near the crack tip. The circles represent pairs of points (1, 2, 3, and 4) used for calculating the CTOA at particular predetermined (constant) positions on the profile. The triangles show the bounds that limit the data used for analysis.

Single Edge Notch Tension Testing: The single edge notch tensile [SEN(T)] test provides a measure of fracture toughness with constraints similar to those observed in pipelines during service. This test, as developed by the researchers at SINTEF Materials Technology, will enable us to determine the ductile-to-brittle transition temperature for pipeline material to provide fracture toughness properties for high-strength steel pipeline materials.

The new controller for the servo-hydraulic load frame on which the SEN(T) tests will be conducted has been installed. At the time of installation, it was recognized that the load signal was extremely noisy, due to a 3-stage manifold with oversized accumulators for dynamic work which were on the machine. Therefore, the machine was retrofitted with a single-stage manifold and the machine will be calibrated early in the next quarter. At that time the system will be ready to commence testing with the four dummy specimens that will be used to develop test procedures without loss of essential material. Actual test specimens are in the process of being prepared.

Modeling:

The CTOA modeling effort described in the last quarterly report continues and will be reported on in the next quarterly report. In addition, Steve Mates and Richard Fields of the NIST Metallurgy Division are continuing their efforts in high strain rate modeling. Their progress follows:

Predicting High Rate Fracture Behavior of Pipeline Steels from Low Rate Fracture Tests and High Rate Plasticity Measurements: This aspect of the program supplements the measurements of CTOA to include effects of rate and temperature on fracture energy. It is well known that the CTOA or CTOD quantifies the kinematic aspects of the ductile fracture process while the rate and temperature behavior of the steel's plasticity control the dynamics. This plasticity can be measured separately from the CTOA or CTOD using the compression Kolsky bar method. Many investigators have shown that the J-integral, the work of fracture, and the dynamic tear energy scale with the product of the flow stress and the CTOD. To date, Kolsky bar tests have been run at room temperature and at -20°C on all the pipeline steels in this program. The room temperature strain rate sensitivity has been determined as well for all these steels. The determination of the strain rate sensitivity at -20°C awaits quasi-static test results that will be available in the next quarter. This data is being used to develop families of stress-strain curves that are functions of strain rate and temperature for all the pipeline steels included in this program. These curves may be combined with the CTOA or CTOD results to predict the generalized strain energy release rate for a propagating crack at any speed and temperature.

The strain rate sensitivity of several grades of pipeline steel have been investigated at the service temperature of the pipeline (-20°C) using a Kolsky Bar technique at NIST Gaithersburg. For a running ductile fracture in a gas pipeline, the ability of a steel to strengthen near the crack tip, where the strain rate is very high, has an important impact on the propagation and arrest behavior of the fracture. The strength of steel generally increases with decreasing temperature, as shown in figure 15, below. This, in turn, will lead to a decrease in the strain rate sensitivity of steel compared to its room temperature behavior. To quantify this effect, the flow stress of pipeline steels were measured in compression at -20°C and at strain rates of 2500 s^{-1} using a Kolsky Bar. The results of these tests will be used to model the fracture behavior of different steels to determine whether high strength steels can be designed to provide both high strength and enhanced strain rate strengthening capacity for optimal fracture resistance at realistic pipeline service temperatures.

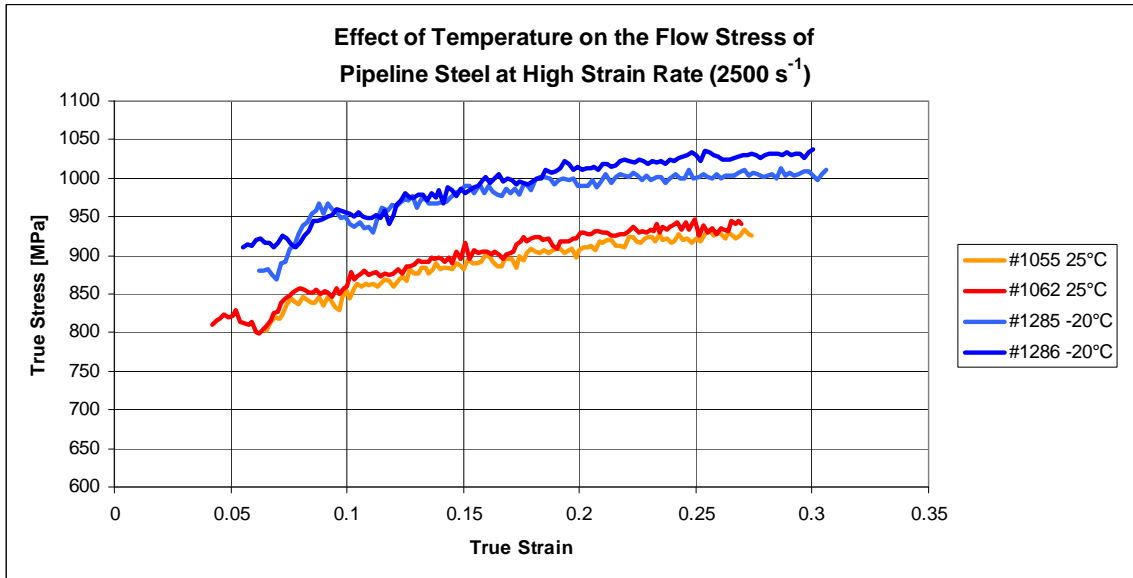


Figure 15. Effect of temperature on flow stress of X65 steel at high strain rates.

Task 4: CTOA Fracture Surface Evaluation

We have completed the dynamic CTOA test plan (0.003, 0.03, 0.3, and 3 m/s rates). Differences in the fracture appearance for X65 and X100 CTOA specimens are observed, as noted in the last quarterly report.

The evaluation of CTOA specimens from quasi static and dynamic tests show 2 typical modes for fracture, referred to here as flat fracture and slant fracture (see figure 16). In the case of flat fracture, the fracture initiates near the center of the specimen thickness, forms an internal void, and final fracture occurs by linking the internal void to the outside surface of the plate by void coalescence on shear planes. This produces a failure with an appearance much like the cup-cone failure for a tensile test specimen (see outlined profile in figure 16). For a slant fracture, the macroscopic plane of failure is on a shear plane through the full thickness of the specimen. Again, fracture initiates in the center region of the specimen, but in this case initiation and growth to failure occurs exclusively on a single macro shear plane (slant). The ductile fracture features observed show a mixture of ductile fracture morphologies on the slant shear fracture surface.

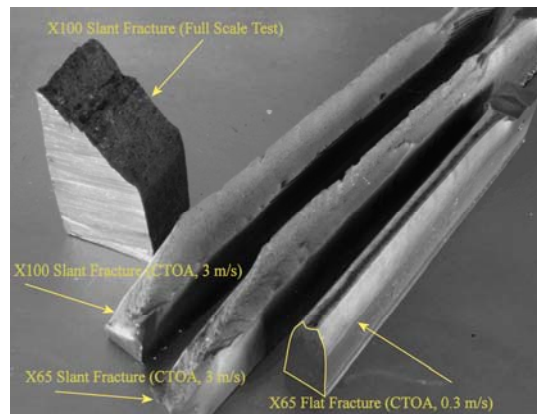


Figure 16. Examples of macroscopic fracture modes for X100 and X65 pipeline steel.

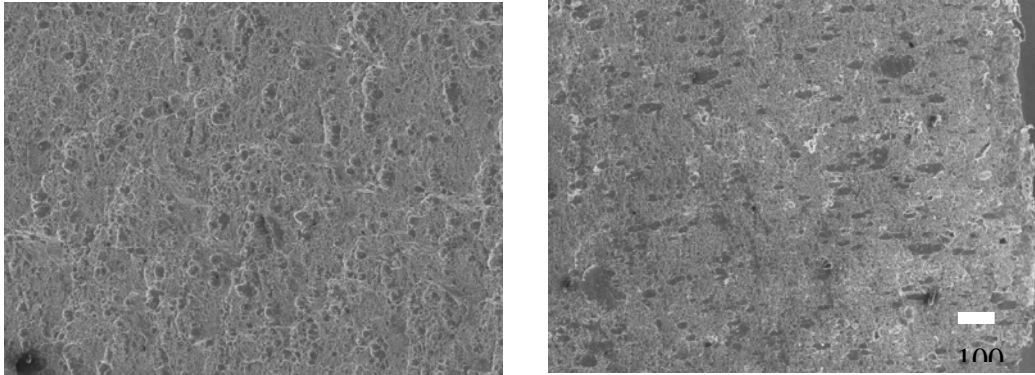


Figure 17. The shape of the larger ductile dimples on the fracture surface is indicative of the local condition for failure in the specimen. This X100 CTOA specimen has slant fracture morphology, but the dimple shapes are round near the center of the plate thickness (left photo), and oval near the surface of the specimen (right).

The macro fracture mode for the full scale tests on the X100 alloy appear to be a combination of flat and shear failure modes. The fracture surface for the full scale test has shear regions on each side of a flat region, but the shear is all on one plane, unlike the example for flat fracture in Figure 16. Possibly even the slant mode fractures initiate on a flat fracture plane, however small, but initial evaluations of the slant CTOA specimens indicate 3 zones for fracture (each having a width of about 1/3 the specimen thickness). As shown in Figure 17, round dimple shapes are present on the center third of the specimen thickness, and oval dimple shapes are present in the 2 zones adjacent to the outside surface of the specimen.

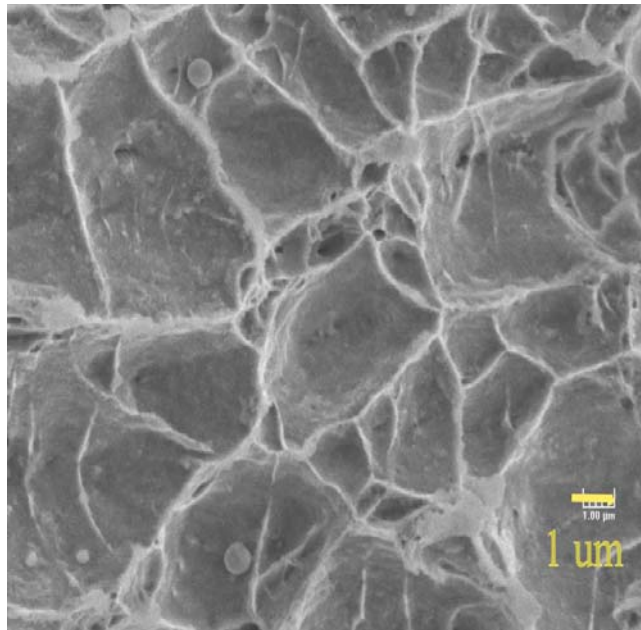


Figure 18. The details of the ductile dimple are typical in the center regions of the X65 CTOA specimens,. On flat fractures the dimples have more depth than those for slant fracture modes.

Figure 18 shows the details of the ductile dimple in the center region of an X65 steel. Flat fracture specimens typically have more depth in the ductile dimples than those that have a slant fracture.

Details of fractures for the CTOA specimens tested at 3 m/s (the fastest rate tested) do not show the flat fracture region observed for the full scale tests of the X100 pipe steel. In

the full scale pipe tests, the flat region has quasi-cleavage like features that are likely related to a high rate fracture mechanism (100 m/s). Apparently we did not reach the velocity necessary to initiate this alternate fracture mechanism in the X100 steel. However, our CTOA specimens were not full thickness (constraint difference) and the microstructure at the center of the pipe thickness was not at the center of the CTOA specimen (sampling difference), so these factors may also play a role in the observed differences in fracture mechanisms.

The X65 and X100 CTOA specimens always failed in a full slant mode at the fastest rates tested (3 m/s). From this result we are tempted to conclude that a critical crack propagation rate is required to produce the full slant failure in these specimens. However, full slant failure modes for both materials are also observed in some of our very slow rate CTOA tests (quasi-static). So, at present, the influence of velocity on the macroscopic failure mode is not clear.

Work on fracture characterization is on schedule and will be concluded for the final report.

Task 5: Method for determination of yield strength in high strength pipeline steels and welds

We are initiating a new test program, focusing on the X100 pipeline steels, designed to help us to better understand the yield-strength behavior of these high strength steels. The program will test round tensile specimens that have ¼-, 3/8-, and ½-inch diameter gauge sections. The material will not be flattened, to avoid Bauschinger effects. Furthermore, the ¼-inch diameter specimens will originate from the upper and lower half of the through thickness. The test matrix is designed to determine if location and sampling size influence the yield strength. Material from two X100 sources will be tested for comparison. We received the specimens for this task late this quarter and will start testing early next quarter.

Task 6: Other tasks

Standards activities:

In addition to supporting this effort through laboratory research, NIST representatives have attended PSIA meetings, reviewed proposals and peer-reviewed projects as needed. We are co-organizing and plan to contribute 2 presentations to an ASTM E08 Workshop, scheduled for the May 2008 meeting in Denver Colorado. The focus will be on standardization of CTOA measurements, and we will contribute our experience and recommendation concerning measurement on pipeline steels. Our dynamic results will also be of interest to the group.

Papers and conferences this reporting quarter:

We submitted 5 abstracts on our efforts to the International Pipeline Conference to be held in September 2008. The abstracts were accepted and full length drafts will be prepared for presentation and publication. The titles of the papers are:

Fracture Morphology and CTOA: X65 and X100 Pipeline Steels

C.N. McCowan, Ph. Darcis, A. Shtechman, E.S. Drexler, R. Reuven, M. Treinen, R. Smith, J. Merritt, T.A. Siewert, J.D. McColskey and R.P Fields

IPC

Effects of Specimen Geometry on Fatigue-Crack Growth Rates in Pipeline Steels

J. M. Treinen, Ph.. P. Darcis, R. Smith, and J. Merritt, J. D. McColskey

IPC

Dynamic CTOA Measurements of Pipeline Steels

A. Shtechman, C.N. McCowan, R. Reuven, Ph. Darcis, E. Drexler, M. Treinen, T.A. Siewert, R. Smith, J. Merritt, and J.D. McColskey

IPC

CTOA Results for X65 and X100 Pipeline Steels: Influence of Displacement Rate

R. Reuven, E. Drexler, A. Shtechman, C. McCowan, Ph. Darcis, M. Treinen, T. Siewert, R. Smith, J. Merritt, and D. McColskey

IPC

CTOA Measurements of Welds in X100 Pipeline Steel

E.S. Drexler, Ph.P. Darcis, C.N. McCowan, J.M. Treinen, A. Shtechman, R. Reuven, T.A. Siewert, R. Smith, J. Merritt, and J.D. McColskey

IPC

Reporting

This is the sixth quarterly report under agreement number DTPH56-06-X-000029. The next quarterly report will be submitted in 3 months.